

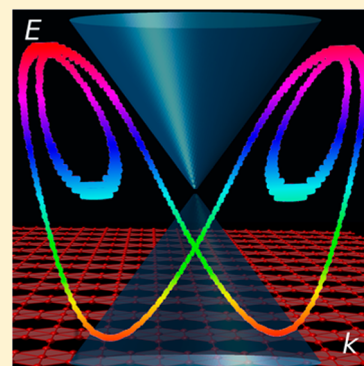
Dirac Cones and Nodal Line in Borophene

Sunny Gupta, Alex Kutana,¹ and Boris I. Yakobson*

Department of Materials Science and Nanoengineering, Rice University, Houston, Texas 77005, United States

Supporting Information

ABSTRACT: Two-dimensional single-layer boron (borophene) has emerged as a new material with several intriguing properties. Recently, the β_{12} polymorph of borophene was grown on Ag(111), and observed to host Dirac fermions. Similar to graphene, β_{12} borophene can be described as atom-vacancy pseudoalloy on a closed-packed triangular lattice; however, unlike graphene, the origin of its Dirac fermions is yet unclear. Here, using first-principles calculations, we probe the origin of Dirac fermions in freestanding and Ag(111)-supported β_{12} borophene. The freestanding β_{12} sheet hosts two Dirac cones and a topologically nontrivial Dirac nodal line with interesting Dirac-like edge states. On Ag(111), the Dirac cones develop a gap, whereas the topologically protected nodal line remains intact, and its position in the Brillouin zone matches that of the Dirac-like electronic states seen in the experiment. The presence of nontrivial topological states near the Fermi level in borophene makes its electronic properties important for both fundamental and applied research.



Graphene, a two-dimensional (2D) polymorph of carbon with a honeycomb lattice has created a plethora of research activities in the past decade. The material hosts massless Dirac fermions and exhibits exotic electronic properties such as high carrier mobility,¹ ambipolar field-effect,² and quantum Hall effect.³ The success of graphene has motivated researchers to look for other 2D materials, where exotic quantum particles such as Majorana, Dirac, and Weyl fermions, sought after in high-energy physics, could be realized in condensed matter systems.

Boron, which lies next to carbon in the periodic table, is found to exist in multiple phases as nanotubes,⁴ clusters,⁵ nanocages (fullerene), and 3D solids.⁶ Recently, two-dimensional monoelemental single-layer boron (borophene) has emerged as a new material,⁸ attracting great attention in the research community.⁹ Following initial theoretical predictions,^{10,11} and subsequent theoretical works performing comprehensive explorations of freestanding and metal substrate-mediated 2D boron phases,^{12–14} several boron monolayer sheets have been experimentally synthesized.^{7,8,15,16} Among them, the β_{12} borophene polymorph was grown on Ag(111), and its Dirac fermion states observed.¹⁵ This experimental work reported¹⁵ that “Dirac points were located”, agreeing with earlier theoretical predictions.¹⁷ The Dirac cones are positioned ~ 2 eV above the Fermi level in freestanding β_{12} ; however, the Dirac-like states were experimentally observed at ~ 0.25 eV below the Fermi level in β_{12} grown on Ag(111).¹⁵ Although Ag(111) substrate acts as electron donor, the charge transfer may not be sufficient to account for the Dirac-like states observed below the Fermi level in β_{12} on Ag(111). Thus, the origin and nature of Dirac cone in the β_{12} sheet remains an open question.

Here, we perform first-principles density functional theory (DFT) calculations to gain insights into the nature of Dirac

cones in the β_{12} sheet in freestanding form and on Ag(111) substrate. Our calculations show that the material hosts two doubly degenerate (4-fold degenerate including spin) Dirac cones above the Fermi level (E_F), at ~ 2 eV and ~ 0.45 eV. The nature and origin of these cones are confirmed by analyzing the symmetry and Berry curvature. Interestingly, the material is also found to host a Dirac nodal line, extending from the Fermi level to ~ 2.2 eV below. The Dirac nodal line^{18–22} in energy-momentum space is a locus of intersection points (nodes) of two dispersion surfaces representing the bands of different orbital symmetry. This 1D band crossing is different from the 0D crossing resulting in a Dirac cone or Dirac and Weyl semimetals. When placed on the Ag(111) substrate, the Dirac cones become gapped, whereas the symmetry-protected nodal line remains intact and extends throughout the BZ, just as in freestanding borophene. The line is thus identified as a likely source of Dirac cone-like features in the experimental ARPES spectra of β_{12} borophene on Ag(111).¹⁵ In order to understand the topological character of the nodal line, edge states are calculated. The edge states demonstrate nontrivial topological nature, adding to a number of interesting electronic properties of β_{12} borophene. These properties could be useful in exploring the physics of topologically nontrivial low-dimensional Dirac materials, and potentially utilized in high-speed electronics.

Boron has one electron less than carbon, and is unstable in a freestanding honeycomb graphene-like lattice.¹⁰ Addition of more boron atoms to the honeycomb lattice can stabilize the structure and result in rich polymorphism. One of the polymorphs, known as the β_{12} sheet, has a planar structure with stripes of filled and empty hexagons alternating along the

Received: February 28, 2018

Accepted: May 9, 2018

Published: May 9, 2018



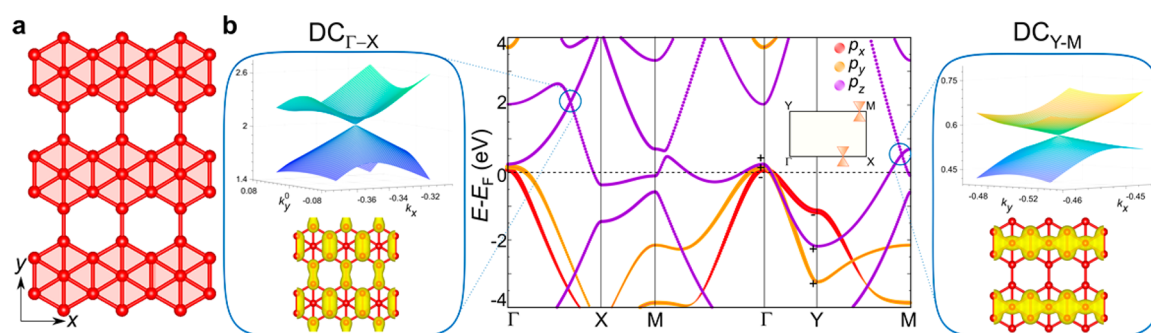


Figure 1. (a) Atomic structure of β_{12} sheet of boron. (b) Central panel: the band structure of freestanding β_{12} sheet with color coded orbital character of bands. Inset shows the location of Dirac cones in the BZ. The parity of p_x , p_y , and p_z bands under in-plane mirror reflection symmetry (σ_v), which takes x , to $-x$ at Γ and Y points are shown. Left panel: a 3D view of the Dirac cone ($DC_{\Gamma-X}$) with a band decomposed isocharge density (BDICD) plot calculated for the lower energy band at the nodal point. Right panel: 3D view of the Dirac cone (DC_{Y-M}) with BDICD plot.

armchair direction (Figure 1a). It has three inequivalent sites with 4-, 5-, and 6- center B–B bonds. Its band structure shows a nearly filled σ band derived from p_x , p_y orbitals, while the π band derived from the p_z orbital is partially filled, as shown in Figure 1b. Interestingly, three bands touch at a single point on the Γ – Y line at E_F , demonstrating a 3-fold (6-fold including spin) degeneracy and may host unconventional quasiparticles predicted recently.^{23,24} Similar to graphene, the bands above E_F have mainly p_z character. A Dirac cone-like band crossing at ~ 2 eV above E_F , labeled as $DC_{\Gamma-X}$ in Figure 1b, can be seen at 2/3 distance from Γ along the Γ – X direction. Dirac cones due to linear band dispersion hosts massless fermions, and the value of Berry curvature diverges at the node, where band crossing occurs.²⁵ Berry curvature $F(k)$ gives a local description of the geometric properties of the wave function and is given by $F(k) = \frac{\partial}{\partial k_x} a_y(k) - \frac{\partial}{\partial k_y} a_x(k)$ where $a_i(k) = -i\psi(k) \left| \frac{\partial}{\partial k_i} \right| \psi(k)$ is called the Berry connection.²⁵ To confirm that this band crossing is a Dirac cone, we calculated the Berry curvature, which was indeed found to diverge at the node, thereby confirming the Dirac dispersion of the band (for detailed methodology, see Supporting Information). We also plotted a 3D band structure to visualize the cone around the nodal point. The slope of the band in the k_x direction is ~ 7.2 eV \AA , equivalent to a Fermi velocity (v_{fx}), $\partial E/\partial k_x = 0.17 \times 10^6$ m/s. In the k_y direction, the slope of the band equals ~ 2.5 eV \AA ($v_{fy} = 0.6 \times 10^5$ m/s), compared to 34 eV \AA ($v_f = 0.83 \times 10^6$ m/s) in graphene when approaching the Dirac point along the Γ – K line. The anisotropy of the Dirac cones along different directions at the nodal point implies direction-dependent electronic properties. To understand the physical origin of this Dirac cone, band decomposed charge density was calculated for the lower energy band at the nodal point (Figure 1b). The charge density distribution is derived from the out-of-plane p_z orbital and is localized only at the hexagon corners with no contributions from the central atom. The resultant structure is like a honeycomb lattice of boron, and the Dirac cone is similar to that observed in graphene. This Dirac cone is significantly away from E_F and the electrical properties associated with the cone would not be easily accessible in experiments.

Interestingly, the material also hosts another Dirac cone, seen as band crossing at ~ 0.45 eV above E_F near the M point along the Y – M direction, labeled as DC_{Y-M} in Figure 1b. Berry curvature was calculated to confirm the Dirac-like dispersion at the band crossing point, and a 3D band structure was plotted to visualize the cone. At DC_{Y-M} , bands have a linear dispersion

equivalent to a Fermi velocity of $\sim 0.19 \times 10^6$ m/s and $\sim 0.39 \times 10^5$ m/s in the k_x , k_y directions, respectively. Similar to $DC_{\Gamma-X}$, DC_{Y-M} is anisotropic along different directions at the nodal point, implying direction-dependent electronic properties. This Dirac cone is also derived from p_z orbitals; however, the origin is completely different. The band decomposed charge density calculated for the lower energy band at the nodal point shows that the contribution to the cone comes only from the central atoms of the hexagon, as shown in Figure 1b. The lattice appears as one-dimensional stripes of boron atoms disconnected from each other. This Dirac cone is close to E_F , and the electrical properties resulting from the Dirac nature could be accessible in experiments.

Apart from the two Dirac cones, the band structure has another interesting feature. The p_z band lies above the p_y and p_x bands close to E_F along the Γ – X direction (Figure 1b). However, along the Y – Γ direction, the order of bands is inverted, i.e., p_x lies above the p_z and p_y bands. The parity of p_x , p_y , and p_z bands under mirror reflection symmetry (σ_v), which takes x (y) to $-x$ ($-y$), are -1 ($+1$), $+1$ (-1), and $+1$ ($+1$), respectively. The electronic wave functions are eigenstates of σ_v with even ($+$) or odd ($-$) parity. The inversion in band character at Γ and Y points in the Brillouin zone is directly manifested in the inverted parity and is shown in Figure 1b. This peculiar feature where parity of bands is inverted in different regions of the BZ leads to an interesting topology of the electronic structure and guarantees band crossing in the energy-momentum space of the crystal as long as the σ_v symmetry is preserved in the lattice. An inversion in band ordering can be seen in the band structure of β_{12} sheet calculated along k_x at k_y ($2\pi/b$) = 0.15 (Figure 2a). The p_z band crosses both p_x and p_y bands at two nodal points. The nodal points extend throughout the energy-momentum space and form a nodal loop with a peculiar topology similar to a knot (Figure 2b). This particular topology has not been seen in any other material and is unique to β_{12} borophene. The bands near the nodal points have a linear dispersion, and this 1D band crossing is called a Dirac nodal line.^{18–22} It is different from the 0D crossing resulting in a Dirac cone, where bands cross only at a point. A 3D band structure was calculated to visualize the band crossing responsible for the nodal line (Figure 2c). The line extends from $(k_x(2\pi/a), k_y(2\pi/b)) = (0, 0.07)$ to $(0.13, 0.5)$, as shown in Figure 2b. The nodal line does not remain at the same energy, but ranges from ~ 0 to ~ 2.2 eV below E_F . The constant energy contours calculated at different energies crossing the nodal line has a dog bone shape as shown in

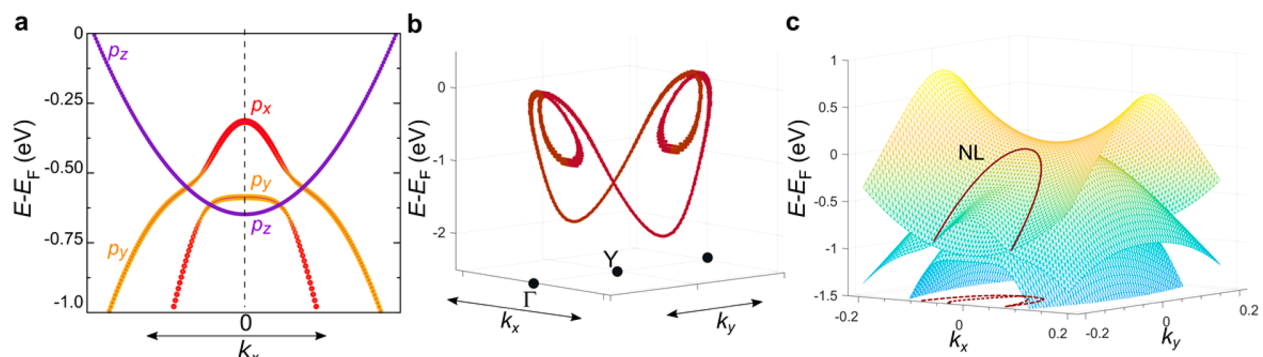


Figure 2. (a) Band structure of freestanding β_{12} sheet calculated along k_x (at k_y , $(2\pi/b) = 0.15$), showing the inversion in the character of bands. This inversion results in band crossing and two nodal points. (b) The nodal points extend throughout the 3D energy-momentum space and form a closed loop with a peculiar topology similar to a knot. (c) 3D band structure showing the band crossing responsible for the nodal line (NL) (marked by magenta solid line). The projection of the location of the nodal line on the k_x - k_y plane (dotted line) is also shown.

Figure S1 (Supporting Information). This shape is peculiar to the nodal line seen in bulk materials.¹⁹ The Dirac nodal lines are similar to topological Dirac semimetal, where two bands having different quantum numbers intersect. Since the bands belong to different subspaces, no mixing is allowed between them, protecting the crossing points to remain gapless. Similarly, in the β_{12} sheet, the crossing between bands of different symmetry leads to an interesting nontrivial topology of electronic states, which will be discussed later.

2D boron sheets were theoretically predicted^{13,26} to form on a metal substrate due to stabilization of sp^2 hybridization by metal passivation. Recently, β_{12} sheet was experimentally synthesized on Ag(111) substrate.^{8,15} Through ARPES measurements they showed that the material hosts Dirac fermions at ~ 0.25 eV below E_F .¹⁵ In our calculations for a freestanding β_{12} sheet, we see that the material hosts two Dirac cones ($DC_{\Gamma-X}$, DC_{Y-M}) and a nodal line. Since any of these elements could result in Dirac-like dispersion, the exact origin of the Dirac fermions seen in the experiment is not clear. To understand the interaction with the substrate, we placed boron on Ag(111). The top layer of Ag(111) has a hexagonal symmetry, and the β_{12} sheet can adopt different orientations, and a proper orientation needs to be determined. Since the growth of boron sheet is epitaxial on Ag(111), only a few orientations are permissible. In experiments,^{8,15} a moiré pattern was seen for a β_{12} sheet grown on Ag(111). This particular pattern corresponds to the hexagons in the β_{12} sheet oriented parallel to the hexagons in Ag(111) (see Figure S2, Supporting Information). In our calculation, we construct a slab geometry, where a β_{12} sheet is placed over a few layers of Ag(111). The computations require the structure to be periodic in all the three directions. A vacuum of 20 Å was placed to separate the periodic images in the z -direction. To match the lattice in the x - y plane, a very large unit cell needs to be constructed. Alternatively, if the boron lattice is rotated by 30° , a very small unit cell with 5 boron atoms is sufficient.

Our calculations show that the interaction of Ag on boron does not depend on the orientation of the two lattices. So, we first consider the structure where the lattices are rotated with respect to each other by 30° (Figure 3a). The lattice parameter of Ag was optimized with LDA functional. The boron lattice was matched with Ag by applying a small biaxial compression of $\sim 1.4\%$. The band structure of the resulting slab geometry is shown in Figure 3b. The states near E_F have contributions from both Ag and B atoms. On comparing the band structure of the

slab with freestanding β_{12} sheet (Figure 1b), one can see that boron bands are significantly perturbed due to interaction with Ag substrate. The out-of-plane p_z orbital interacts strongly with Ag and is modulated the most. The Dirac cones ($DC_{\Gamma-X}$, DC_{Y-M}) observed in the freestanding β_{12} sheet can also be seen in the band structure of the slab. The location of both cones in the BZ remains the same; however, they develop a gap and shift down in energy due to perturbation from Ag, as shown by black arrows in Figure 3b. The identity of both cones was confirmed by calculating the band decomposed charge density and comparing the symmetry of corresponding bands with that of $DC_{\Gamma-X}$, DC_{Y-M} in the free-standing sheet. The gapped nature of cones was also ascertained by calculating the band structure with a dense 500 k -point sampling along the Γ -X and Y-M directions. $DC_{\Gamma-X}$ develops a gap of ~ 150 meV, while DC_{Y-M} is significantly perturbed, and the Dirac-like dispersion almost disappears. The in-plane p_x and p_y bands are found to be less perturbed compared to the p_z bands. The p_x and p_y bands near Γ point move down in energy from the position near E_F in the free-standing sheet to ~ 0.3 eV below E_F , as shown by the green arrow in Figure 3b. This energy shift corresponds to electron doping of boron by Ag substrate. To confirm that doping by Ag indeed shifts the boron bands down by ~ 0.3 eV, a jellium slab was placed on top of boron. A shift in the boron bands by ~ 0.3 eV correspond to a doping of 0.3 e⁻/cell ($\sim 2 \times 10^{14}$ /cm²) to boron by Ag. Moreover, a shift in ~ 0.3 eV is also close to the difference in the work function (~ 0.4 eV) of freestanding β_{12} sheet and Ag(111). The calculated electrostatic potential profile for β_{12} sheet on Ag(111) also confirms doping of B by Ag (Figure S3, Supporting Information).

The band structure of β_{12} on Ag(111) retains the nodal line of the freestanding sheet. The band structure of the slab shows a band crossing at ~ 0.25 eV below E_F near the Γ point along Γ -X, as shown by the blue arrow in Figure 3b. The crossing is between the p_z and p_y bands of boron along Γ -X, while it is between the p_z and p_x bands along Γ -Y. The bands have a linear dispersion and form a nodal line. Unlike the Dirac cones, the nodal line is not gapped by placing on Ag substrate and is protected due to σ_v symmetry. This nodal line is slightly different from that seen in the free-standing sheet. In the slab, the nodal line first appears along the Γ -X direction, while it is seen along Γ -Y in the free-standing sheet. This is because the β_{12} sheet is slightly strained ($\sim 1.4\%$) when placed on Ag. The p_x band, which was below p_z at the Γ point in the unstrained sheet moves up in energy in the strained sheet and crosses each

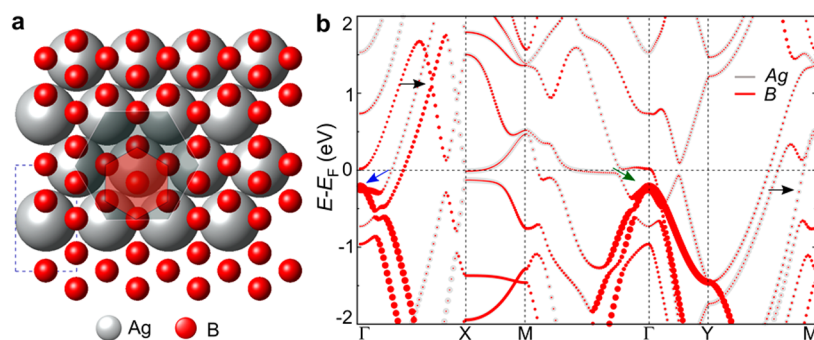


Figure 3. (a) Slab geometry of a β_{12} sheet placed over Ag(111). The unit cell is marked by a dashed blue rectangle. The hexagons in Ag and B lattice are rotated by 30° with respect to each other and are shaded in black and red color, respectively. (b) The band structure of the slab with Ag and B bands shown in gray and red color, respectively. The black arrows point to the location of Dirac cones $DC_{\Gamma-X}$ and DC_{Y-M} seen in the freestanding sheet. $DC_{\Gamma-X}$ develops a gap ~ 150 meV, while DC_{Y-M} is significantly perturbed. Green arrow near the Γ point shows the shift in boron bands by ~ 0.3 eV when placed on Ag(111), which corresponds to a doping of ~ 0.3 e^- /cell. Blue arrow at ~ 0.25 eV below E_F shows the location of band crossing along $\Gamma-X$, which forms a nodal line in the BZ.

other along $\Gamma-X$. This can be clearly seen in the band structure of free-standing strained boron sheet (see Figure S4, Supporting Information). The nodal line extends in energy from ~ 0.25 eV to ~ 1.75 eV below E_F . In a recent experimental study, the β_{12} sheet was shown to host Dirac fermions.¹⁵ A Dirac-like dispersion of bands was seen with the nodal point at ~ 0.25 eV below E_F . The nodal line in β_{12} borophene on Ag(111) emerges at ~ 0.25 eV below E_F in our calculations, leading to the possibility of its cross-section being observed in the experiment.

To confirm that the Dirac-like dispersions seen in the experiment were due to a nodal line, we next considered the slab geometry, where the β_{12} sheet is parallel to the Ag lattice (Figure S2, Supporting Information). A large unit cell with 140 boron atoms was constructed to match the orientation with Ag lattice. The band structure was calculated and then folded to the BZ of boron to compare with results of 30° rotated geometry (Figure S5, Supporting Information). The band structures look similar, demonstrating that the interaction of Ag on boron does not depend on the orientation of the two lattices. A similar band crossing resulting in a nodal line can be seen at ~ 0.25 eV below E_F along the $\Gamma-X$ direction. The orientation of the β_{12} sheet with respect to Ag is known, hence we can predict the band unfolding from boron to Ag BZ (see Supporting Information for details of band unfolding). The area of boron BZ is found to be half of Ag BZ, so the M point in Ag BZ will fold to the Γ point in boron BZ (Figure S6, Supporting Information). Since the portion of the $\Gamma-X$ line in the BZ of β_{12} sheet is mapped to the M-K line of Ag BZ, the band crossing that is seen along the $\Gamma-X$ direction of the BZ of β_{12} sheet must unfold to the location near the M point along the MK line of the Ag BZ. This matches exactly in both energy and momentum with the nodal point and Fermi pockets seen centered on the M point in the Ag BZ in experiment,¹⁵ thereby confirming that the Dirac-like dispersion seen in the experiment is due to the nodal line in the β_{12} sheet.

Nodal line materials belong to the family of topological metals/semimetals with nontrivial band topologies. There are different ways to check the nontrivial topological character of the bands such as²⁷ (i) compute topological invariant for the line nodes along which two nondegenerate bands touch, (ii) use adiabatic continuity arguments to connect the unknown band structure to a known topological or nontopological band structure, and (iii) directly compute the spectrum of surface or

edge states. A bulk/2D topological material interfaced with vacuum changes the topological number at the interface and requires the existence of topologically protected surface/edge states. Hence, the existence of surface/edge states in a topologically nontrivial bulk/2D material is guaranteed by bulk-boundary correspondence considerations²⁸ and is sufficient to probe the trivial/nontrivial topological nature of nodal line. In topological nodal line materials, the surface/edge states must connect the nodal lines/points. To compute the edge spectrum, we consider semi-infinite nanoribbons with both armchair and zigzag edges. In our case, nodal line is seen in both free-standing β_{12} sheets as well when placed on Ag in the slab geometry. Here, we consider only the free-standing sheet for edge states calculation. The violet regions in Figure 4 represent the spectral weight of bulk bands, whereas the white curves represent the edge states of the armchair edge (see Figure S7, Supporting Information for edge states of zigzag edge). The edge states are found to connect the nodal points, signifying the nontrivial topological nature of the material. Interestingly the edge states have a Dirac-like dispersion shown by the white arrow in Figure 4. These edge states are different from the drumhead type surface states seen in bulk topological nodal line materials and are unique to the β_{12} sheet. Up to now, many nodal line materials have been discovered in bulk phases;^{18–21} however, only a few have been found in the 2D flatland.^{22,29} The nontrivial topological properties are intrinsic to borophene, yet, until now, the β_{12} sheet has been grown only on Ag(111), whose additional electronic states may obscure the topological properties of the β_{12} sheet. Therefore, for practical observation, the material must typically be either exfoliated or grown on nonmetals. Experiments are underway³⁰ to reveal the nature of borophene-metal bonding, to potentially ease exfoliation.

The nodal line in a free intrinsic β_{12} sheet spans ~ 2.2 eV in energy (Figure 2b), with the Fermi level positioned at its very top. At any hole-doping, shifting the Fermi level down this range, there exist linearly dispersive bands. Thus, different sections of the nodal line can be “accessed” through either chemical or electrostatic gate-doping. Based on the electronic DOS, the number of carriers required to shift the Fermi level can be estimated as ~ 0.27 h^+ /eV/atom (h^+ means a hole) and is shown in the Figure S8 (Supporting Information). In order to access the entire nodal line, doping in the range 0–0.6 h^+ /atom is required. We also calculated the work functions of

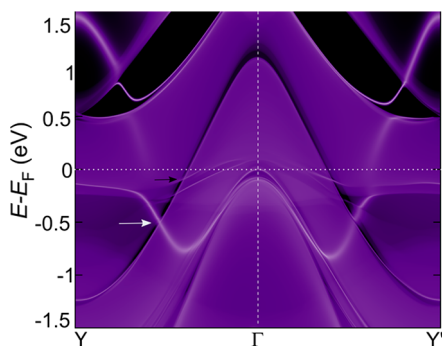


Figure 4. Bloch spectrum of a free-standing β_{12} sheet ribbon with an armchair edge. The violet color represents contributions from bulk atoms, while white bands depict contributions from edge atoms. White and black arrows point to Dirac like edge states and nodal points, respectively.

(111) surfaces of several elemental metals and β_{12} -borophene (Figure S9, Supporting Information) to estimate possible levels of doping. Assuming the Fermi level of borophene being set by the metal substrate, p -doping with Fermi level shift of ~ 1 eV could be possibly achieved with a high work function metal such as Pt. The nontrivial electronic structure of β_{12} borophene belongs to a broader class called topological metals, such as type-II Dirac and Weyl materials,³¹ where topological band crossing occurs near E_F in the presence of additional electronic states at the same energy. The metallicity arises from tilting of bands, while in the absence of tilt, the band crossing will be at a constant energy. Due to additional metallic bands and the 2D nature of β_{12} borophene, various electronic properties (distinct phase shift in Shubnikov–de Haas (SdH) oscillation,³² chiral anomaly,³³ and chiral Landau levels³⁴), which arise from the nontrivial electronic structure, may be concealed in β_{12} borophene. However, some of the properties resulting from topologically nontrivial states should still be observable. Linearly dispersive topologically protected bands of β_{12} borophene should give rise to distinctly observable high carrier mobility and linear transverse magnetoresistance. In topologically trivial metals, magnetoresistance $\rho \sim H^2$ is quadratic with applied magnetic field, whereas it is linear $\rho \sim H$ in systems with linear energy spectrum.³⁵ Thus, linear positive magnetoresistance signifies the linearly dispersive bands near the Fermi level. Moreover, due to additional hole pockets from normal parabolic bands and electron pockets from linear Dirac bands (Figure 1b, 2c) at E_F , large magnetoresistance due to electron–hole resonances should arise in β_{12} borophene (similar to a previous report on WTe_2 ³⁶). This is of broad interest for magnetic memory³⁷ and sensing³⁸ applications. For device applications, the nodal line states should yield high carrier mobility, a prediction that is verifiable in experiments.

Additionally, recent experiments have demonstrated that exotic superconductivity with p -wave pairing can be realized in Dirac-type materials Cd_3As_2 ,^{39,40} and graphene.⁴¹ Given that pristine β_{12} sheet was predicted to possess intrinsic superconductivity with large electron–phonon coupling at long phonon wavelength,^{17,42,43} and also has topological band crossing at the Fermi level, interorbital Cooper pairing between electrons of different quantum numbers with p -wave symmetry can arise.^{44,45} Further, p -wave superconductivity has been predicted to host Majorana fermions, which are essential for creating fault-tolerant quantum computers.⁴⁶ Of course, to affirm the possibility of p -wave superconductivity in a β_{12} sheet,

an exact calculation of electron–phonon coupling constant and Coulomb pseudopotential with s - and p -like symmetry must be carried out, calling for further theoretical explorations. Moreover, p -wave superconductivity manifests in zero bias conductance peaks,⁴⁴ and, for experimental verification, point contact spectroscopy measurements must be done.

In summary, using first-principles calculations, we predict topologically nontrivial electronic states in the β_{12} sheet of boron. The material host two Dirac-cones and a nodal line. The Dirac cones develop a gap when placed on Ag(111), while the nodal line remains protected. The nodal line extends in energy from ~ 0.25 to ~ 1.75 eV below E_F and has a dog-bone shaped constant energy contour. This suggests that the Dirac-like dispersion seen in a recent experiment is due to the nodal line. The nodal line is topologically nontrivial and is uniquely associated with Dirac-like edge states. The linear dispersion of edge states is unique to boron and is different from the usual drumhead-like surface states seen in bulk topological nodal line materials. Our DFT simulation and theoretical analysis demonstrate the origin of Dirac-like states and topological nodal-line fermions in boron and pave the way for exploring the exotic properties of topological nodal-line states in low-dimensional condensed matter systems with possible applications in magnetic memory, high-speed electronics, and topological superconductivity.

■ ASSOCIATED CONTENT

Supporting Information

The Supporting Information is available free of charge on the ACS Publications website at DOI: 10.1021/acs.jpcllett.8b00640.

Methodology, constant energy contour, slab geometry with hexagons in boron lattice parallel to Ag(111), electrostatic potential profile, details for band folding from Ag(111) to boron BZ, Bloch spectrum for zigzag edge, doping levels required for shifting E_F , and work functions of various (111) metal surfaces compared with β_{12} sheet (PDF)

■ AUTHOR INFORMATION

Corresponding Author

*E-mail: biy@rice.edu.

ORCID

Alex Kutana: 0000-0001-6405-6466

Notes

The authors declare no competing financial interest.

■ ACKNOWLEDGMENTS

We acknowledge the support by the Army Research Office (W911NF-16-1-0255) and by the Office of Naval Research (N00014-15-1-2372). S.G. would like to thank Dr. Sharmila N. Shirodkar and Dr. Evgeni S. Penev for helpful discussions. The authors acknowledge the DAVinCI - Center for Research Computing at Rice University and DoD HPCMP for computational resources.

■ REFERENCES

- (1) Novoselov, K. S.; Geim, A. K.; Morozov, S. V.; Jiang, D.; Katsnelson, M. I.; Grigorieva, I. V.; Dubonos, S. V.; Firsov, A. A. Two-Dimensional Gas of Massless Dirac Fermions in Graphene. *Nature* 2005, 438, 197–200.

- (2) Novoselov, K. S.; Geim, A. K.; Morozov, S. V.; Jiang, D.; Zhang, Y.; Dubonos, S. V.; Grigorieva, I. V.; Firsov, A. A. Electric Field Effect in Atomically Thin Carbon Films. *Science* **2004**, *306*, 666–669.
- (3) Novoselov, K. S.; McCann, E.; Morozov, S. V.; Fal'ko, V. I.; Katsnelson, M. I.; Zeitler, U.; Jiang, D.; Schedin, F.; Geim, A. K. Unconventional Quantum Hall Effect and Berry's Phase of 2π in Bilayer Graphene. *Nat. Phys.* **2006**, *2*, 177–180.
- (4) Boustani, I.; Quandt, A. Nanotubes of Bare Boron Clusters: Ab Initio and Density Functional Study. *EPL Europhys. Lett.* **1997**, *39*, 527.
- (5) Boustani, I. Systematic Ab Initio Investigation of Bare Boron Clusters: Determination of the Geometry and Electronic Structures of B_n ($n = 2-14$). *Phys. Rev. B: Condens. Matter Mater. Phys.* **1997**, *55*, 16426–16438.
- (6) Saxena, S. *Handbook of Boron Nanostructures*; Pan Stanford: New York, 2016.
- (7) Mannix, A. J.; Zhou, X.-F.; Kiraly, B.; Wood, J. D.; Alducin, D.; Myers, B. D.; Liu, X.; Fisher, B. L.; Santiago, U.; Guest, J. R.; et al. Synthesis of Borophenes: Anisotropic, Two-Dimensional Boron Polymorphs. *Science* **2015**, *350*, 1513–1516.
- (8) Feng, B.; Zhang, J.; Zhong, Q.; Li, W.; Li, S.; Li, H.; Cheng, P.; Meng, S.; Chen, L.; Wu, K. Experimental Realization of Two-Dimensional Boron Sheets. *Nat. Chem.* **2016**, *8*, 563–568.
- (9) Zhang, Z.; Penev, E. S.; Yakobson, B. I. Two-Dimensional Boron: Structures, Properties and Applications. *Chem. Soc. Rev.* **2017**, *46*, 6746–6763.
- (10) Tang, H.; Ismail-Beigi, S. Novel Precursors for Boron Nanotubes: The Competition of Two-Center and Three-Center Bonding in Boron Sheets. *Phys. Rev. Lett.* **2007**, *99*, 115501.
- (11) Yang, X.; Ding, Y.; Ni, J. Ab Initio Prediction of Stable Boron Sheets and Boron Nanotubes: Structure, Stability, and Electronic Properties. *Phys. Rev. B: Condens. Matter Mater. Phys.* **2008**, *77*, 041402.
- (12) Penev, E. S.; Bhowmick, S.; Sadrzadeh, A.; Yakobson, B. I. Polymorphism of Two-Dimensional Boron. *Nano Lett.* **2012**, *12*, 2441–2445.
- (13) Liu, Y.; Penev, E. S.; Yakobson, B. I. Probing the Synthesis of Two-Dimensional Boron by First-Principles Computations. *Angew. Chem., Int. Ed.* **2013**, *52*, 3156–3159.
- (14) Zhang, Z.; Yang, Y.; Gao, G.; Yakobson, B. I. Two-Dimensional Boron Monolayers Mediated by Metal Substrates. *Angew. Chem., Int. Ed.* **2015**, *54*, 13022–13026.
- (15) Feng, B.; Sugino, O.; Liu, R.-Y.; Zhang, J.; Yukawa, R.; Kawamura, M.; Iimori, T.; Kim, H.; Hasegawa, Y.; Li, H.; et al. Dirac Fermions in Borophene. *Phys. Rev. Lett.* **2017**, *118*, 096401.
- (16) Li, W.; Kong, L.; Chen, C.; Gou, J.; Sheng, S.; Zhang, W.; Li, H.; Chen, L.; Cheng, P.; Wu, K. Experimental Realization of Honeycomb Borophene. *Sci. Bull.* **2018**, *63*, 282–286.
- (17) Penev, E. S.; Kutana, A.; Yakobson, B. I. Can Two-Dimensional Boron Superconduct? *Nano Lett.* **2016**, *16*, 2522–2526.
- (18) Burkov, A. A.; Hook, M. D.; Balents, L. Topological Nodal Semimetals. *Phys. Rev. B: Condens. Matter Mater. Phys.* **2011**, *84*, 235126.
- (19) Bian, G.; Chang, T.-R.; Sankar, R.; Xu, S.-Y.; Zheng, H.; Neupert, T.; Chiu, C.-K.; Huang, S.-M.; Chang, G.; Belopolski, I.; et al. Topological Nodal-Line Fermions in Spin-Orbit Metal $PbTaSe_2$. *Nat. Commun.* **2016**, *7*, 10556.
- (20) Neupane, M.; Belopolski, I.; Hosen, M. M.; Sanchez, D. S.; Sankar, R.; Szlawska, M.; Xu, S.-Y.; Dimitri, K.; Dhakal, N.; Maldonado, P.; et al. Observation of Topological Nodal Fermion Semimetal Phase in $ZrSiS$. *Phys. Rev. B: Condens. Matter Mater. Phys.* **2016**, *93*, 201104.
- (21) Gupta, S.; Juneja, R.; Shinde, R.; Singh, A. K. Topologically Nontrivial Electronic States in $CaSn_3$. *J. Appl. Phys.* **2017**, *121*, 214901.
- (22) Feng, B.; Fu, B.; Kasamatsu, S.; Ito, S.; Cheng, P.; Liu, C.-C.; Feng, Y.; Wu, S.; Mahatha, S. K.; Sheverdyaeva, P.; et al. Experimental Realization of Two-Dimensional Dirac Nodal Line Fermions in Monolayer Cu_2Si . *Nat. Commun.* **2017**, *8*, 1007.
- (23) Ezawa, M. Triplet Fermions and Dirac Fermions in Borophene. *Phys. Rev. B: Condens. Matter Mater. Phys.* **2017**, *96*, 035425.
- (24) Bradlyn, B.; Cano, J.; Wang, Z.; Vergniory, M. G.; Felser, C.; Cava, R. J.; Bernevig, B. A. Beyond Dirac and Weyl Fermions: Unconventional Quasiparticles in Conventional Crystals. *Science* **2016**, *353*, aaf5037.
- (25) Xiao, D.; Chang, M.-C.; Niu, Q. Berry Phase Effects on Electronic Properties. *Rev. Mod. Phys.* **2010**, *82*, 1959–2007.
- (26) Liu, H.; Gao, J.; Zhao, J. From Boron Cluster to Two-Dimensional Boron Sheet on Cu(111) Surface: Growth Mechanism and Hole Formation. *Sci. Rep.* **2013**, *3*, 3238.
- (27) Bansil, A.; Lin, H.; Das, T. Colloquium: Topological Band Theory. *Rev. Mod. Phys.* **2016**, *88*, 021004.
- (28) Hasan, M. Z.; Kane, C. L. Colloquium: Topological Insulators. *Rev. Mod. Phys.* **2010**, *82*, 3045–3067.
- (29) Zhang, H.; Xie, Y.; Zhang, Z.; Zhong, C.; Li, Y.; Chen, Z.; Chen, Y. Dirac Nodal Lines and Tilted Semi-Dirac Cones Coexisting in a Striped Boron Sheet. *J. Phys. Chem. Lett.* **2017**, *8*, 1707–1713.
- (30) Campbell, G. P.; Mannix, A. J.; Emery, J. D.; Lee, T.-L.; Guisinger, N. P.; Hersam, M. C.; Bedzyk, M. J. Resolving the Chemically Discrete Structure of Synthetic Borophene Polymorphs. *Nano Lett.* **2018**, *18*, 2816–2821.
- (31) Armitage, N. P.; Mele, E. J.; Vishwanath, A. Weyl and Dirac Semimetals in Three-Dimensional Solids. *Rev. Mod. Phys.* **2018**, *90*, 015001.
- (32) Wang, S.; Lin, B.-C.; Wang, A.-Q.; Yu, D.-P.; Liao, Z.-M. Quantum Transport in Dirac and Weyl Semimetals: A Review. *Adv. Phys. X* **2017**, *2*, 518–544.
- (33) Zyuzin, A. A.; Burkov, A. A. Topological Response in Weyl Semimetals and the Chiral Anomaly. *Phys. Rev. B: Condens. Matter Mater. Phys.* **2012**, *86*, 115133.
- (34) Zhu, Z.; Winkler, G. W.; Wu, Q.; Li, J.; Soluyanov, A. A. Triple Point Topological Metals. *Phys. Rev. X* **2016**, *6*, 031003.
- (35) Abrikosov, A. A. Quantum Magnetoresistance. *Phys. Rev. B: Condens. Matter Mater. Phys.* **1998**, *58*, 2788–2794.
- (36) Ali, M. N.; Xiong, J.; Flynn, S.; Tao, J.; Gibson, Q. D.; Schoop, L. M.; Liang, T.; Haldolaarachchige, N.; Hirschberger, M.; Ong, N. P.; et al. Large, Non-Saturating Magnetoresistance in WTe_2 . *Nature* **2014**, *514*, 205–208.
- (37) Moritomo, Y.; Asamitsu, A.; Kuwahara, H.; Tokura, Y. Giant Magnetoresistance of Manganese Oxides with a Layered Perovskite Structure. *Nature* **1996**, *380*, 141–144.
- (38) Lenz, J. E. A. Review of Magnetic Sensors. *Proc. IEEE* **1990**, *78*, 973–989.
- (39) Kobayashi, S.; Sato, M. Topological Superconductivity in Dirac Semimetals. *Phys. Rev. Lett.* **2015**, *115*, 187001.
- (40) Wang, H.; Wang, H.; Liu, H.; Lu, H.; Yang, W.; Jia, S.; Liu, X.-J.; Xie, X. C.; Wei, J.; Wang, J. Observation of Superconductivity Induced by a Point Contact on 3D Dirac Semimetal Cd_3As_2 Crystals. *Nat. Mater.* **2016**, *15*, 38–42.
- (41) Di Bernardo, A.; Millo, O.; Barbone, M.; Alpern, H.; Kalcheim, Y.; Sassi, U.; Ott, A. K.; De Fazio, D.; Yoon, D.; Amado, M.; et al. p -Wave Triggered Superconductivity in Single-Layer Graphene on an Electron-Doped Oxide Superconductor. *Nat. Commun.* **2017**, *8*, 14024.
- (42) Gao, M.; Li, Q.-Z.; Yan, X.-W.; Wang, J. Prediction of Phonon-Mediated Superconductivity in Borophene. *Phys. Rev. B: Condens. Matter Mater. Phys.* **2017**, *95*, 024505.
- (43) Cheng, C.; Sun, J.-T.; Liu, H.; Fu, H.-X.; Zhang, J.; Chen, X.-R.; Meng, S. Suppressed Superconductivity in Substrate-Supported β_{12} Borophene by Tensile Strain and Electron Doping. *2D Mater.* **2017**, *4*, 025032.
- (44) Sato, M.; Ando, Y. Topological Superconductors: A Review. *Rep. Prog. Phys.* **2017**, *80*, 076501.
- (45) Wan, X.; Savrasov, S. Y. Turning a Band Insulator into an Exotic Superconductor. *Nat. Commun.* **2014**, *5*, 4144.
- (46) Wilczek, F. Majorana Returns. *Nat. Phys.* **2009**, *5*, 614.